Development of Chronic Bronchitis and Emphysema in β-Epithelial Na^+ Channel–Overexpressing Mice

Marcus A. Mall[1], Jack R. Harkema[2], Joanna B. Trojanek[1], Diana Treis[1], Alessandra Livraghi[3], Susanne Schubert[1], Zhe Zhou[1], Silvia M. Kreda[3], Stephen L. Tilley[4], Elizabeth J. Hudson[3], Wanda K. O'Neal[3], and Richard C. Boucher[3]

[1]Pediatric Pulmonology and Cystic Fibrosis Center, Department of Pediatrics III, University of Heidelberg, Heidelberg, Germany; [2]Department of Pathobiology and Diagnostic Investigation, Michigan State University, East Lansing, Michigan; and [3]Cystic Fibrosis/Pulmonary Research and Treatment Center and [4]Division of Pulmonary and Critical Care Medicine, Department of Medicine, School of Medicine, The University of North Carolina at Chapel Hill, Chapel Hill, North Carolina

Rationale: **Chronic obstructive pulmonary disease is a leading cause of death worldwide, but its pathogenesis is not well understood. Previous studies have shown that airway surface dehydration in β-epithelial Na^+ channel (βENaC)–overexpressing mice caused a chronic lung disease with high neonatal pulmonary mortality and chronic bronchitis in adult survivors.**

Objectives: **The aim of this study was to identify the initiating lesions and investigate the natural progression of lung disease caused by airway surface dehydration.**

Methods: **Lung morphology, gene expression, bronchoalveolar lavage, and lung mechanics were studied at different ages in βENaC-overexpressing mice.**

Measurements and Main Results: **Mucus obstruction in βENaC-overexpressing mice originated in the trachea in the first days of life and was associated with hypoxia, airway epithelial necrosis, and death. In surviving βENaC-overexpressing mice, mucus obstruction extended into the lungs and was accompanied by goblet cell metaplasia, increased mucin expression, and airway inflammation with transient perinatal increases in tumor necrosis factor-α and macrophages, IL-13 and eosinophils, and persistent increases in keratinocyte-derived cytokine (KC), neutrophils, and chitinases in the lung. βENaC-overexpressing mice also developed emphysema with increased lung volumes, distal airspace enlargement, and increased lung compliance.**

Conclusions: **Our studies demonstrate that airway surface dehydration is sufficient to initiate persistent neutrophilic airway inflammation with chronic airways mucus obstruction and to cause transient eosinophilic airway inflammation and emphysema. These results suggest that deficient airway surface hydration may play a critical role in the pathogenesis of chronic obstructive pulmonary diseases of different etiologies and serve as a target for novel therapies.**

Keywords: chronic obstructive lung disease; epithelial Na^+ channels; airway surface liquid; inflammation; mucus

AT A GLANCE COMMENTARY

Scientific Knowledge on the Subject

Airway surface dehydration is a key feature of cystic fibrosis and produces chronic bronchitis in mice. The initiating lesions and the natural history of lung disease caused by airway surface dehydration have not been elucidated.

What This Study Adds to the Field

Airway surface dehydration is sufficient to initiate persistent neutrophilic airway inflammation with chronic airways mucus obstruction and to cause transient eosinophilic airway inflammation and emphysema. These results suggest that deficient airway surface hydration may play a critical role in the pathogenesis of chronic obstructive pulmonary diseases of different etiologies and serve as a target for novel therapies.

Cystic fibrosis (CF) lung disease is the most common genetic form of chronic obstructive pulmonary disease (COPD) and is caused by mutations in the cystic fibrosis transmembrane conductance regulator (CFTR) gene (1, 2), which encodes a protein that is a cAMP-dependent Cl^- channel and regulates the epithelial Na^+ channel (ENaC) (3–6). In CF airway epithelia, CFTR-mediated Cl^- secretion is defective, and ENaC-mediated Na^+ absorption is increased (7–9). *In vitro* studies of primary human airway cultures suggested that these defects in vectorial ion transport resulted in airway surface liquid (ASL) volume depletion and adhesion of dehydrated mucus, which was predicted to impair normal ciliary function and efficient mucus clearance in CF airways (10). To further elucidate the role of ASL volume depletion in the *in vivo* pathogenesis of CF, we have previously generated a mouse model with airway-specific overexpression of ENaC (11). In this mouse model, we demonstrated (*1*) that overexpression of the β-subunit of ENaC (encoded by the *Scnn1b* gene) under control of the Clara cell secretory protein (CCSP) promoter was sufficient to increase airway Na^+ absorption *in vivo*, (*2*) that elevated airway Na^+ absorption caused ASL volume depletion and reduced mucus clearance, and (*3*) that deficient mucus clearance produced spontaneous lung disease sharing key features with CF and other forms of COPD, including substantial pulmonary mortality and airway mucus obstruction, goblet cell metaplasia, chronic neutrophilic inflammation, and impaired clearance of bacterial pathogens (11).

Together, the results from these *in vitro* and *in vivo* studies demonstrate that ASL volume depletion is a key mechanism in the pathogenesis of CF lung disease. Furthermore, cigarette smoke has recently been shown to decrease CFTR expression and cAMP-dependent Cl^- secretion *in vitro* and in nasal respiratory epithelia of cigarette smokers *in vivo* (12). These data indicate that impaired ASL volume regulation may also be implicated in the pathogenesis of cigarette smoke–induced chronic bronchitis. The aim of the present study was to define the initial pulmonary lesions and elucidate the sequence of steps in the

(*Received in original form August 21, 2007; accepted in final form December 13, 2007*)

Supported by Marie Curie Excellence Grant from the European Commission (MEXT-CT-2004–013666 to M.A.M.), the Deutsche Forschungsgemeinschaft (DFG MA 2,081/3–2 to M.A.M.), the North American Cystic Fibrosis Foundation (MALL04G0 to M.A.M. and R026-CR02 to W.K.O.), and the National Institutes of Health (NIH SCOR P50 HL60280, P01 HL34322, and MTCC P30 DK065988 to R.C.B.).

Correspondence and requests for reprints should be addressed to Marcus A. Mall, M.D., Pediatric Pulmonology and Cystic Fibrosis Center, Department of Pediatrics III, University of Heidelberg, Im Neuenheimer Feld 153, 69120 Heidelberg, Germany. E-mail: marcus.mall@med.uni-heidelberg.de

This article has an online supplement, which is accessible from this issue's table of contents at www.atsjournals.org

Am J Respir Crit Care Med Vol 177. pp 730–742, 2008
Originally Published in Press as DOI: 10.1164/rccm.200708-1233OC on December 13, 2007
Internet address: www.atsjournals.org

in vivo pathogenesis of COPD consequent to airway surface dehydration in βENaC-overexpressing mice. A focus was on the relationships between ASL volume depletion and mucus obstruction, the presumed cause of mortality in this model. To achieve this goal, we performed quantitative longitudinal studies from fetal to adult ages of the pulmonary phenotype, including airway mucus obstruction, goblet cell metaplasia, mucin gene expression, airway inflammation, lung volume, alveolar size, and pulmonary function. The results of our studies yielded novel insights into the role of airway surface dehydration in the *in vivo* pathogenesis of CF and possibly other forms of COPD and identified targets for novel therapeutic strategies for the treatment of these diseases. Some of the results of this study have been previously reported in the form of abstracts (13, 14).

METHODS

Experimental Animals

All animal studies were approved by the animal care and use committees of the relevant institutions. The generation of βENaC-overexpressing mice (line 6608) has been described previously (11). Further details on experimental animals are provided in the online supplement.

Bronchoalveolar Lavage Cell Counts and Cytokine Measurements

Bronchoalveolar lavage (BAL) was obtained and cell counts were determined as previously described (11). Macrophage size was determined as described in the online supplement. Concentrations of tumor necrosis factor (TNF)-α, keratinocyte-derived cytokine (KC), and IL-13 were measured by ELISA (R&D Systems, Minneapolis, MN) or with a Cytometric Bead Array Mouse Inflammation kit (BD Biosciences, San Diego, CA).

Morphology

Lungs and tracheae were fixed, paraffin embedded, sectioned, and stained with hematoxylin and eosin (H&E) or Alcian blue periodic acid-Schiff as previously described (11). For transmission electron microscopy (TEM) studies, lungs were fixed and processed, and ultrastructural tissue examination was performed as described in the online supplement.

Airway Morphometry

Tracheae were sectioned longitudinally, and lungs were sectioned transversally at the level of the proximal intrapulmonary main axial airway near the hilus and at the distal intrapulmonary axial airway. Airway mucus obstruction was assessed by determining mucus volume density as previously described (15). Airway epithelial glycogen content, epithelial height, and numeric cell densities of goblet cells and degenerative airway epithelial cells were determined as described in the online supplement.

Lung Volume and Mean Linear Intercepts

Lungs were inflated with 4% buffered formalin to 25 cm of fixative pressure, and lung volumes were determined by the volume displacement method (16). Lungs were processed for histology, sectioned, and stained with H&E. Mean linear intercepts were determined as previously described (17). Further details are provided in the online supplement.

Immunohistochemistry

Immunohistochemical staining for Ym1 was performed on formalin-fixed, paraffin-embedded lung sections using rabbit polyclonal anti-Ym1 antibody (18) as described in the online supplement.

Hypoxia Detection in the Lung

Tissue hypoxia was assessed by intraperitoneal injection of 3-d-old neonatal mice with pimonidazole hydrochloride (Hypoxyprobe-1; Chemicon, Temecula, CA) and immunostaining of frozen lung sections using fluorescein isothiocyanate–labeled monoclonal antibody (MAb) 1 (Hypoxyprobe-1 Plus Kit; Chemicon) as described in the online supplement.

Blood Gas Analyses

Blood gas measurements in neonatal mice (3–5 d) were performed using a blood gas analyzer (Radiometer ABL 500; Diamond Diagnostics, Holliston, MA) as described in the online supplement.

Western Blotting

Acidic mammalian chitinase (AMCase) protein expression was assessed in cell-free BAL fluid (BALF) from βENaC-overexpressing mice and wild-type littermates by Western blotting using an anti-AMCase rabbit serum (19) as described in the online supplement.

Real-time Reverse Transcriptase–Polymerase Chain Reaction

Quantitative reverse transcriptase–polymerase chain reaction for Muc5ac, Muc5b, Muc4, Gob5, eotaxin-1, IL-13, IFN-γ, Ym1, Ym2, AMCase, and β-actin was performed on an Applied Biosystems 7500 Real Time PCR System using TaqMan universal polymerase chain reaction master mix and inventoried TaqMan gene expression assays (Applied Biosystems, Darmstadt, Germany) as described in the online supplement. Relative fold changes in target gene expression between βENaC-overexpressing mice and wild-type littermates were determined by normalization to expression of the reference gene β-actin as previously described (20).

Pulmonary Function Studies

Invasive measurements of lung mechanics were performed in anesthetized and paralyzed 8-week-old adult mice using a computer-controlled small animal ventilator (Flexi Vent system; Scireq, Montreal, PQ, Canada) to determine dynamic resistance, dynamic compliance, pressure–volume curves, and static compliance of the lung, as previously described (21, 22).

Statistics

Data were analyzed with SigmaStat version 3.1 (Systat Software, Erkrath, Germany) and are reported as mean ± SEM. Statistical analyses were performed using Student's *t* test, Mann-Whitney rank sum test, one-way analysis of variance, Kruskal-Wallis analysis of variance on Ranks, or chi-square test as appropriate, and $P < 0.05$ was accepted to indicate statistical significance.

RESULTS

ASL Volume Depletion–induced Mucus Obstruction, Goblet Cell Metaplasia, and Mucus Hypersecretion

To identify the onset and temporal evolution of goblet cell metaplasia, mucus hypersecretion, and mucus obstruction caused by ASL volume depletion, we performed longitudinal morphometric studies and studies on airway mucin expression in fetal (Embryonic Day [E] 18.5), newborn (Postnatal Day [PN] 0.5), neonatal (PN 3.5), juvenile (1–3 wk of age), and adult (6 wk of age) βENaC-overexpressing mice and littermate control mice. The onset of mortality in βENaC-overexpressing mice commenced at 3 d of age with an overall mortality of approximately 50% in the first 2 weeks of life (Figure 1A). Compared with wild-type (Figure 1B), mortality at 3 days was associated with light microscopic evidence of tracheal plugging (Figures 1C and 1D), increased mucus volume density (Figure 1E), and mucus plugging of the larynx (Figure 1F) but not goblet cell metaplasia (Figure 1G). The extent of tracheal and laryngeal mucus obstruction was significantly more severe in age-matched deceased compared with βENaC-overexpressing mice killed as part of this study (Figure 1F), indicating that death occurred due to mucus obstruction of the glottis and subsequent asphyxia. In contrast, neither intrapulmonary airway mucus obstruction nor goblet cell metaplasia were detected in the lungs from fetal, newborn (data not shown), or neonatal (PN 3.5) βENaC-overexpressing mice (Figures 2A, 2G, and 2I).

In 2-week-old surviving βENaC-overexpressing mice, intraluminal mucus plugging extended into intrapulmonary airways

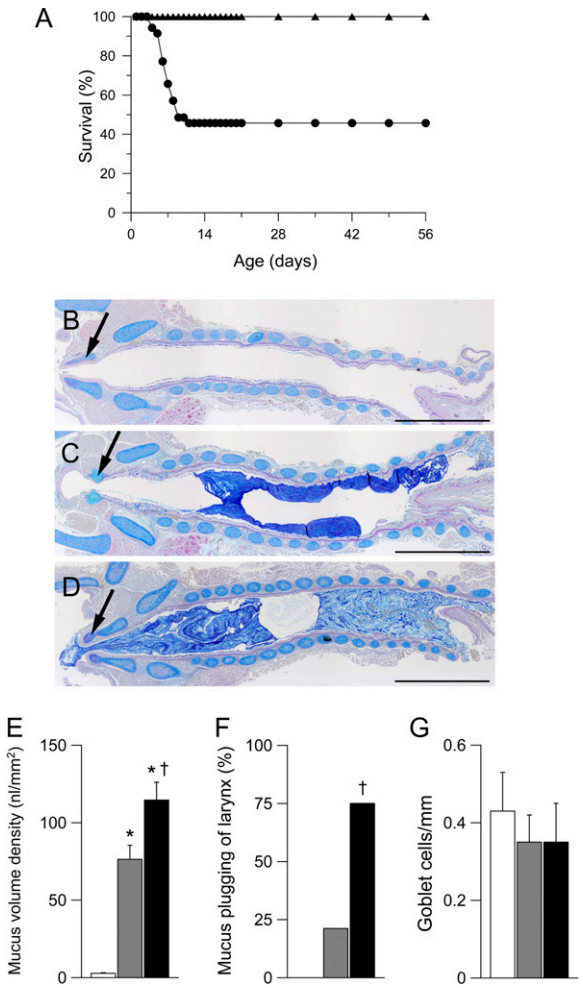

Figure 1. Pulmonary mortality and tracheal mucus obstruction in β-epithelial Na^+ channel (βENaC)–overexpressing mice. (*A*) Survival curves from βENaC-overexpressing mice (*circles*; n = 35) and wild-type littermates (*triangles*; n = 36). (*B–D*) Histology (Alcian blue periodic acid-Schiff) of tracheae from wild-type (*B*) and βENaC-overexpressing mice (*C*) killed at the age of 3 days and a βENaC-overexpressing mouse that died spontaneously at 4 days (*D*). Larynx is indicated by *arrows*. *Scale bars*, 1,000 μm. Representative for n = 6–14 mice per group. (*E–G*) Summary of tracheal mucus content as determined from volume density measurements (*E*), frequency of laryngeal mucus plugging (*F*), and goblet cell counts (*G*) in tracheae from wild-type (*open bars*), βENaC-overexpressing mice killed at 3 days (*shaded bars*), and βENaC-overexpressing mice that died spontaneously at the ages of 3 to 7 days (*solid bars*). n = 11 – 16 mice per group. *$P < 0.001$ versus wild-type. †$P < 0.01$ versus killed βENaC-overexpressing mice.

(Figure 2). Mucus obstruction was most prominent in proximal intrapulmonary main axial airways (large-diameter bronchiole; Figures 2B and 2G) but also extended into the more distal conducting airways (small-diameter, preterminal bronchioles; Figures 2C and 2H) and persisted in 3- and 6-week-old βENaC-overexpressing mice (Figures 2D, 2E, 2G, and 2H). In contrast to early tracheal mucus plugging, intrapulmonary airway mucus obstruction was accompanied by goblet cell metaplasia in βENaC-overexpressing mice. Wild-type mice exhibited a transient increase in airway goblet cell numbers that peaked at 2 weeks of age, persisted in proximal main axial airways (large-diameter bronchioles), and waned in the more distal small-diameter bronchioles of adult animals (Figures 2I and 2J). In βENaC-overexpressing mice, goblet cell numbers were significantly increased in proximal large-diameter bronchioles at the age of 3 and 6 weeks and in distal small-diameter bronchioles at all time points (Figures 2I and 2J). The onset of goblet cell metaplasia in 2-week-old βENaC-overexpressing mice was paralleled by epithelial cell hypertrophy with epithelial thickening that persisted in adult animals (Figure 2K).

To explore the relationship between mucus obstruction and goblet cell metaplasia with mucin expression, we determined mRNA transcript levels of the airway mucins Muc5ac, Muc5b, and Muc4 and the goblet cell marker Gob-5 (Clca-3) in lungs from newborn to adult βENaC-overexpressing mice and control mice. In wild-type mice, expression of Muc5ac and Gob-5 was significantly elevated at the age of 1 week, and expression of Muc5b and Muc4 was significantly elevated at the age of 3 weeks when compared with newborn mice (Figures 3A–3D). Although induction of Muc5ac, Muc4, and Gob-5 was transient, with peak levels at 1 and 3 weeks, expression of Muc5b remained elevated in adult wild-type mice (Figures 3A–3D). In βENaC-overexpressing mice, mRNA expression levels of Muc5ac, Muc5b, Muc4, and Gob-5 followed similar time courses and were significantly increased compared with control mice from the age of 3 weeks onward (Figures 3A–3D).

Taken together, these data demonstrate that ASL volume depletion caused airway mucus obstruction, goblet cell metaplasia, and increased mucin gene expression in an age-dependent fashion. In the first week of life, airway Na^+ hyperabsorption caused tracheal mucus plugging and high mortality in the absence of goblet cell metaplasia and elevated mucin gene expression (Figures 1–3). Subsequently, in surviving βENaC-overexpressing mice, mucus obstruction extended into intrapulmonary airways and was accompanied by secondary goblet cell metaplasia and increased mucin expression (Figures 2 and 3).

Mucus Obstruction Causes Hypoxia

Because histologic evaluation identified tracheal mucus obstruction in a large fraction of βENaC-overexpressing mice as early as 3 days (*see* Figures 1C–1F) and because the majority of deaths in βENaC-overexpressing mice occurred in the first week of life (*see* Figure 1A), we performed blood gas analyses in neonatal mice (PN 3.5–5.5) to determine the effects of tracheal mucus plugging on ventilation. These analyses showed that P_{O_2}, oxygen saturation, and base excess were significantly reduced in blood samples from βENaC-overexpressing mice compared with wild-type littermates (Table 1). These results demonstrate that tracheal mucus plugging was sufficient to cause systemic hypoxia. Reduced base excess, in parallel with hypoxia, suggested metabolic compensation of respiratory alkalosis, indicating that respiratory insufficiency was a chronic process in βENaC-overexpressing mice.

Airway Na^+ Hyperabsorption and Epithelial Necrosis

High-resolution light and TEM studies revealed that airway Na^+ hyperabsorption was accompanied by early airway epithelial degeneration and necrosis in the intralobular airways but not in the trachea (Figure 4). Swollen, highly vacuolated, degenerative airway epithelial cells were observed in high numbers in neonatal βENaC-overexpressing mice but rarely in wild-type control mice (Figures 4A and 4B). In βENaC-overexpressing mice, degenerative epithelial cells were absent in the fetus (E 18.5; data not shown), present in newborn mice (PN 0.5), peaked at the age of 3 days, and were rarely observed in the airways of older βENaC-overexpressing animals (Figure 4C). Furthermore, the intraepithelial content of PAS-positive material was reduced in newborn βENaC-overexpressing mice, indicating a reduction in airway epithelial glycogen content compared with wild-type

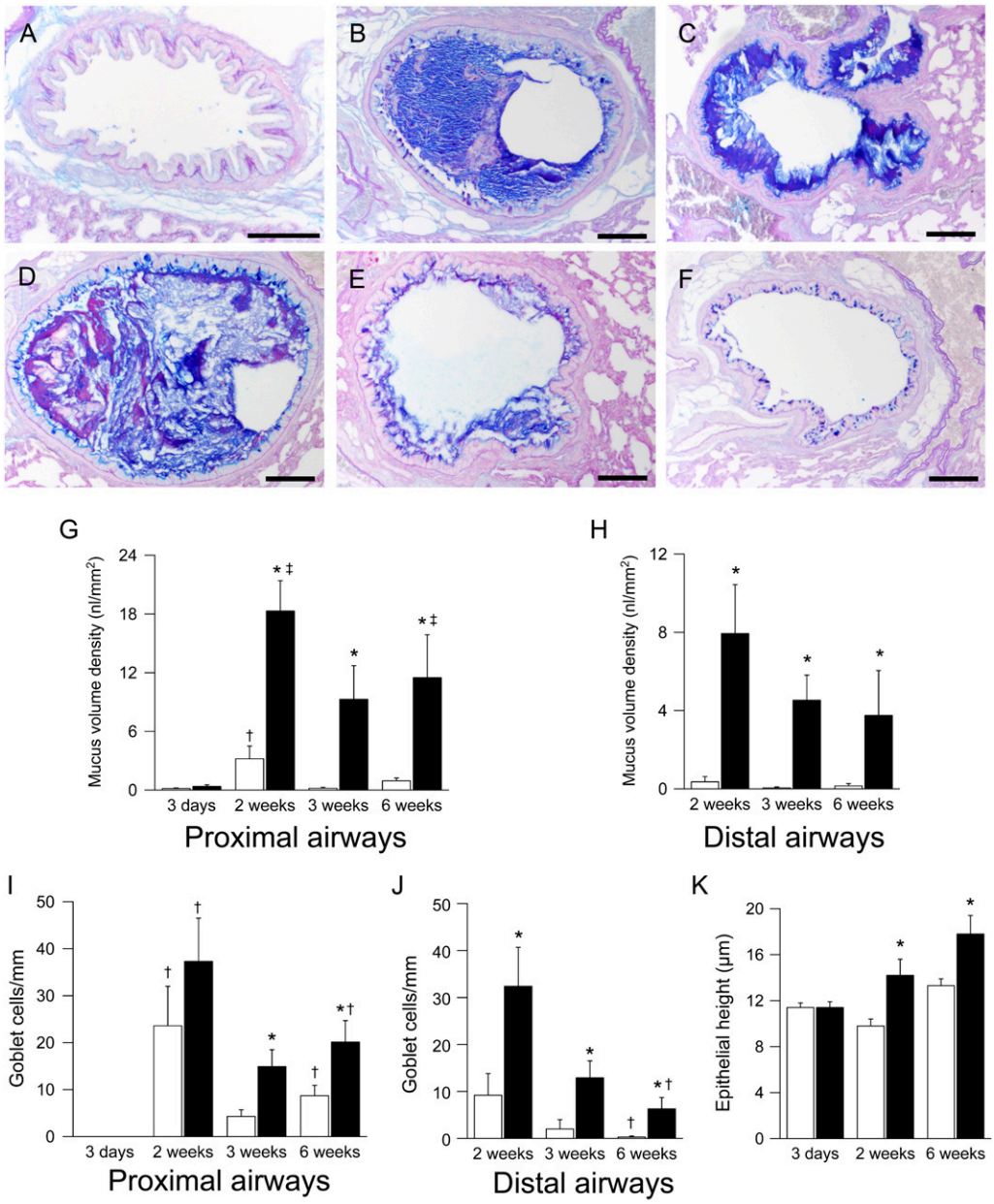

Figure 2. Development of airway mucus obstruction, goblet cell metaplasia, and epithelial hyperplasia in β-epithelial Na^+ channel (βENaC)–overexpressing mice. (*A–D*) Lung histology (Alcian blue periodic acid-Schiff) from βENaC-overexpressing mice that were killed at 3 days (*A*), 2 weeks (*B, C*), and 6 weeks (*D, E*) of age and from a 2-week-old wild-type control mouse (*F*). Lungs were sectioned at the level of the proximal (*B, D*) main axial airway and from the distal axial airway (*E, F*). *Scale bars*, 100 μm. Representative for n = 6–14 mice per group. (*G–K*) Summary of airway mucus obstruction, goblet cell counts, and epithelial height in bronchi from wild-type (*open bars*) and βENaC-overexpressing mice (*solid bars*) at 3 days, 2 weeks, 3 weeks, and 6 weeks of age. n = 6–10 mice per group. (*G*) Mucus content in proximal main axial airways. $*P < 0.01$ versus littermate control mice at same age; $^{\dagger}P < 0.05$ versus 3-day-old and 3-week-old wild-type mice; $^{\ddagger}P < 0.05$ versus 3-day-old βENaC-overexpressing mice. (*H*) Mucus content in distal axial airways. $*P < 0.05$ versus wild-type mice of same age. (*I*) Goblet cell counts in proximal main axial airways. $*P < 0.05$ versus wild-type mice of same age; $^{\dagger}P < 0.05$ versus 3-day-old mice of same genotype. (*J*) Goblet cell counts in distal axial airways. $*P < 0.02$ versus wild-type mice of same age; $^{\dagger}P < 0.05$ versus 2-week-old mice of same genotype. (*K*) Epithelial height in lobar bronchi. $*P < 0.02$ versus wild-type mice.

control mice (Figure 4D). Ultrastructural examination by TEM identified abnormalities in Clara cells but not in ciliated cells. These abnormalities included depletion of epithelial glycogen stores and vacuolarization of the endoplasmatic reticulum, indicative of hydropic degeneration of Clara cells in newborn βENaC-overexpressing but not wild-type mice (Figures 4E and 4F). Compared with wild-type mice (Figure 4G), the majority of degenerative Clara cells of 3-day-old βENaC-overexpressing mice had pyknotic nuclei (Figure 4H), and immunostaining for activated caspase 3 as a marker for apoptosis was negative (data not shown), indicating that these cells underwent necrosis.

To assess a possible role of tissue hypoxia in airway epithelial necrosis, 3-day-old mice were treated with the hypoxia probe pimonidazole hydrochloride, and lung sections were subsequently evaluated by immunofluorescence using monoclonal antibodies that detect protein adducts of this probe in hypoxic cells. Strong immunoreactive signals were detected in the airway epithelium of βENaC-overexpressing mice but not in wild-type littermates (Figure 5). Immunoreactive signals were not detected in alveolar epithelia or in lungs from mice that were not treated with the hypoxia probe in either genotype. These data demonstrate that airway epithelial cells were hypoxic in neonatal βENaC-overexpressing mice and suggest that Clara cell necrosis resulted from cellular hypoxia.

Taken together, these data demonstrate that Na^+ hyperabsorption induced by CCSP promoter–driven overexpression of βENaC resulted in neonatal depletion of glycogen stores, cellular hypoxia, hydropic degeneration, and necrosis of Clara cells. Degenerative and/or necrotic cells were not observed in mouse airways where CCSP promoter-driven overexpression of transgenes did not result in Na^+ hyperabsorption (11) (i.e., in αENaC- and γENaC-overexpressing mice; data not shown). In βENaC-overexpressing mice, necrotic Clara cells were subsequently cleared from the airways and replaced by Clara cells and goblet cells in juvenile and adult βENaC-overexpressing mice (*see* Figures 2B–2E, 4C).

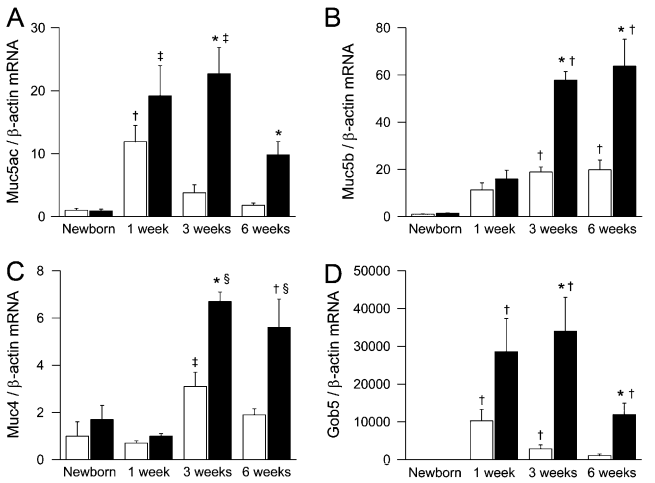

Figure 3. Time course of airway mucin expression in β-epithelial Na^+ channel (βENaC)–overexpressing mice. (*A–D*) Transcripts levels of Muc5ac, Muc5b, Muc4, and Gob5 in lungs from wild-type (*open bars*) and βENaC-overexpressing (*solid bars*) mice at birth, 1 week, 3 weeks, and 6 weeks of age. Data are expressed as fold changes from newborn wild-type mice. n = 6–14 mice per group. (*A*) Muc5ac. $^*P < 0.001$ versus littermate control mice at same age; $^\dagger P < 0.05$ versus newborn, 3-week-old, and 6-week-old wild-type mice; $^\ddagger P < 0.05$ versus newborn βENaC-overexpressing mice. (*B*) Muc5b. $^*P < 0.01$ versus wild-type mice of same age; $^\dagger P < 0.05$ versus newborn mice of same genotype. (*C*) Muc4. $^*P < 0.001$ versus wild-type mice of same age; $^\dagger P < 0.05$ versus wild-type mice of same age; $^\ddagger P < 0.05$ versus newborn and 1-week-old wild-type mice; $^\S P < 0.05$ versus 1-week-old βENaC-overexpressing mice. (*D*) Gob5 expression. $^*P < 0.05$ versus wild-type mice of same age; $^\dagger P < 0.05$ versus newborn mice of same genotype.

Development of Chronic Airway Inflammation

In histologic lung sections, necrotic lesions in the airways of neonatal βENaC-overexpressing mice were accompanied by acute cellular inflammation of large- and small-diameter bronchioles (bronchiolitis), consisting of intramural and intraluminal infiltration of neutrophils and airway luminal macrophages engulfing necrotic cellular debris. To study the evolution of airway inflammation, we performed longitudinal BAL studies in 5-day-old to adult mice and measured the absolute numbers and relative distributions of different inflammatory cell types (Figure 6). BAL macrophages were significantly increased at 5 days and 2 weeks and were normalized in numbers but remained morphologically activated (i.e., hypertrophic cells with highly vacuolated cytoplasm) in 3- and 6-week-old βENaC-overexpressing mice compared with control mice (Figures 6B, 6G–6I). Neutrophils were recruited in parallel with macrophages, peaked at 5 days, and remained significantly elevated at all time points in βENaC-overexpressing mice (Figure 6C). Two- to three-week-old wild-type mice exhibited a transient airway eosinophilia that waned in adult mice, as previously reported (23). Eosinophilia was significantly increased in βENaC-overexpressing mice. In contrast to persistent neutrophilic inflammation, eosinophilia waned in adult βENaC-overexpressing animals (Figure 6D). Lymphocyte counts tended to be higher in βENaC-overexpressing mice than in control mice, but a significant difference was only observed in adult animals (Figure 6E).

We determined protein and/or mRNA expression of proinflammatory cytokines, including TNF-α, KC (Cxcl1), eotaxin-1 (Ccl11), IL-13, and IFN-γ in BAL or lung homogenates from newborn to adult βENaC-overexpressing mice and control mice (Figure 7). None of the cytokines was elevated in fetal (E 18.5) or newborn (PN 0.5) βENaC-overexpressing mice compared with wild-type littermates. TNF-α was transiently elevated in BAL from βENaC-overexpressing mice, with peak levels in neonatal mice (i.e., at the age when necrotic lesions were most prominent) (Figures 4C and 7A). The neutrophil-attracting chemokine KC was significantly elevated in βENaC-overexpressing mice from the first week of life, and increased KC levels were sustained into adulthood (Figure 7B). Expression of the eosinophil-attracting chemokine eotaxin 1 was increased in βENaC-overexpressing mice, but the fold increase over wild-type mice was less pronounced than KC expression (Figure 7C). mRNA expression of the Th2 cytokine IL-13 was transiently induced in neonatal wild-type mice and waned in older animals, indicating that wild-type animals were Th2 biased during development (24) (Figure 7E). In βENaC-overexpressing mice, IL-13 mRNA expression followed the same time course but was significantly increased at all time points compared with control mice. Significantly elevated IL-13 protein levels were observed in 2- to 3-week old mice but not in adult βENaC-overexpressing mice (Figures 7D and 7E). In contrast, mRNA expression of the Th1 cytokine IFN-γ increased with age in wild-type and βENaC-overexpressing mice but did not differ between genotypes at any time point (Figure 7F). Taken together, the transient elevation of IL-13, followed by sustained elevation of IFN-γ mRNA expression, indicated a shift from Th2 toward Th1 response during normal development (24).

Airway Inflammation Is Associated with Expression of Chitinases

In airway mucus plugs of βENaC-overexpressing mice, we frequently observed eosinophilic crystalline material (Figure 8A) similar to that identified as the crystallized product of various members of mammalian chitinase family, including Ym1, Ym2, and AMCase (18, 19, 25, 26). Immunohistochemically, Ym1-positive staining was present in the crystals and in the luminal airway mucus of βENaC-overexpressing mice but not in control mice (Figures 8B and 8C). Positive Ym1 immunostaining was also observed in nonciliated airway epithelial cells (mainly mucous cells) lining proximal large-diameter bronchiolar airways and in macrophages within distal and proximal airway lumens and alveolar airspaces. In contrast, in wild-type littermates, Ym1 protein expression was confined to alveolar macrophages. By TEM, acicular (needle-shaped) crystals were identified in the cytoplasm of macrophages (Figure 8D). Immunohistochemical

TABLE 1. BLOOD GAS ANALYSIS FROM NEONATAL β-EPITHELIAL NA^+ CHANNEL–OVEREXPRESSING MICE AND WILD-TYPE LITTERMATES*

Genotype	pH	P_{CO_2} (*mm Hg*)	P_{O_2} (*mm Hg*)	HCO_3^- (*mmol/L*)	BE (*mmol/L*)	Sat O_2 (%)
Wild-type	7.42 ± 0.01	48.7 ± 1.7	49.9 ± 2.0	30.8 ± 0.6	5.6 ± 0.5	83.7 ± 1.8
βENaC overexpressing	7.40 ± 0.01	48.8 ± 1.4	43.1 ± 2.4†	29.2 ± 0.6	3.8 ± 0.5†	77.0 ± 2.4†

Definition of abbreviations: BE = base excess; βENaC = β-epithelial Na^+ channel; Sat O_2 = O_2 saturation.
* n = 8–14 mice per group.
† $P < 0.05$ compared with littermate control mice.

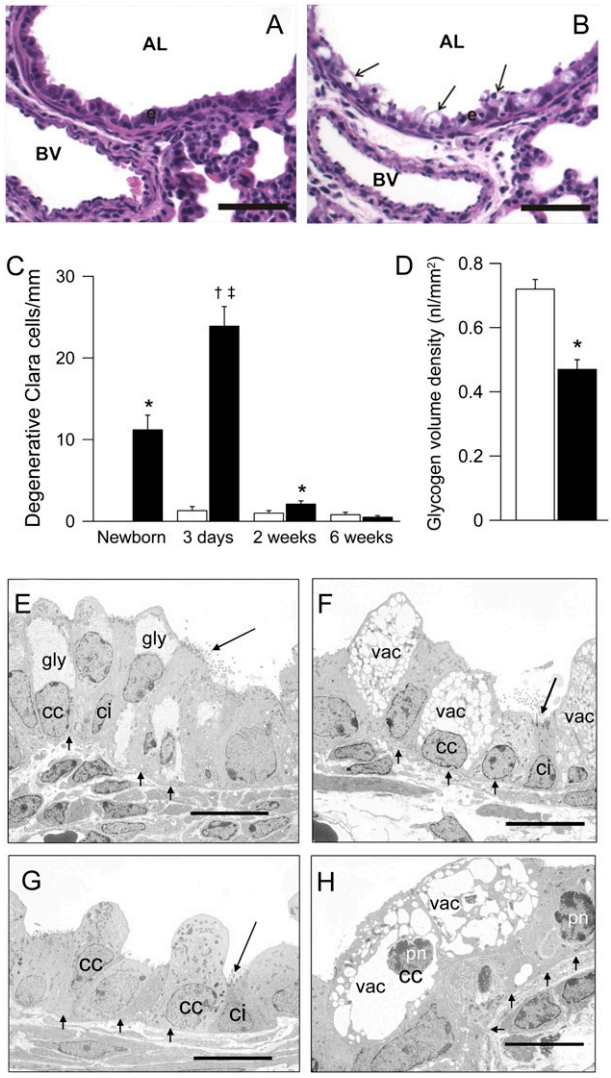

Figure 4. Epithelial degeneration and necrosis in airways of neonatal β-epithelial Na^+ channel (βENaC)–overexpressing mice. (*A, B*) Histology (hematoxylin and eosin) of bronchi from 3-day-old wild-type (*A*) and βENaC-overexpressing (*B*) mice showing hydropic degeneration of airway epithelial cells in βENaC-overexpressing mice (*arrows*). AL = airway lumen; BV = blood vessel; *scale bars*, 50 μm. (*C*) Time course of degenerative Clara cells in bronchi of wild-type (*open bars*) and βENaC-overexpressing (*solid bars*) mice at birth, 3 days, 2 weeks, and 6 weeks of age. n = 4–12 mice per group. $*P < 0.05$ versus wild-type mice of same age; $^{\dagger}P < 0.001$ versus wild-type mice of same age; $^{\ddagger}P < 0.05$ versus newborn, 2-week-old, and 6-week-old βENaC-overexpressing mice. (*D*) Reduced epithelial glycogen, as determined by volume density measurements of periodic acid-Schiff–positive glyconen in newborn βENaC-overexpressing (*solid bars*) compared with wild-type (*open bars*) mice. n = 4–5 mice per group. $*P < 0.001$ versus littermate control mice. (*E–H*) Transmission electron microscopy of airway epithelia in bronchi from newborn (*E, F*) and 3-day-old (*G, H*), wild-type (*E, G*), and βENaC-overexpressing mice (*F, H*). (*F*) Loss of intracellular glycogen (gly) and endoplasmatic reticulum vacuolarization (vac) in Clara cells (cc) but not in ciliated cells (ci) from newborn βENaC-overexpressing mice. (*H*) Pyknotic nuclei (pn) as a sign of necrosis in Clara cells from 3-day-old βENaC-overexpressing mice. *Scale bars*, 10 μm. Representative for n = 4–12 mice per group.

reaction toYm1 was minimal or absent in the lungs of newborn mice, strongest in 3-week-old mice, and waned in adult βENaC-overexpressing mice. Moreover, Western blot analysis revealed increased levels of AMCase in BALF harvested from adult

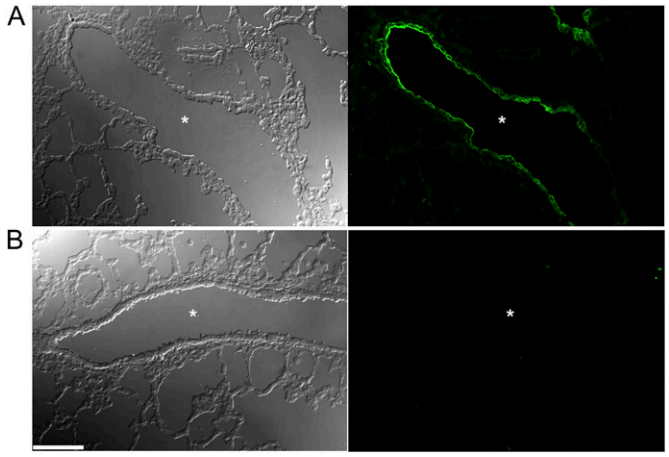

Figure 5. Hypoxia of airway epithelia in neonatal β-epithelial Na^+ channel (βENaC)-overexpressing mice. Tissue hypoxia was determined by injection of 3-day-old neonatal mice with the hypoxia probe pimonidazole hydrochloride, and subsequent immunostaining of lung sections with an antibody that detects the probe in hypoxic cells and evaluation by confocal microscopy. Images depict differential interference contrast microscopy (DIC) (*left panels*) and fluorescein isothiocyanate planes (*right panels*) of lung sections from βENaC-overexpressing (*A*) and wild-type (*B*) mice. Specific immunoreactive signals were observed in the epithelial cells lining the airways of βENaC-overexpressing mice, but not in wild-type lungs (*right panels*). *Asterisks* indicate the position of the airway lumen. *Scale bar*, 100 μm.

βENaC-overexpressing mice in comparison to wild-type littermates (Figure 8E).

To further elucidate the role of Ym1, Ym2, and AMCase in ASL depletion–induced airway inflammation, we determined their longitudinal mRNA expression profiles in lungs from newborn to adult βENaC-overexpressing mice and control mice (Figures 8F–8H). Ym1 transcript levels increased continuously with age in wild-type mice and were significantly increased from the age of 3 weeks in βENaC-overexpressing animals (Figure 8F). In contrast to sustained expression of Ym1, Ym2 transcript levels were only transiently induced in wild-type littermates, with peak levels at 3 weeks and waning in adult mice (Figure 8G). Similar to Ym1, Ym2 expression was significantly increased in 3- and 6-week-old βENaC-overexpressing mice compared with control mice. AMCase expression was not regulated during development in wild-type mice but was significantly increased in 3-week-old and older βENaC-overexpressing mice (Figure 8H). These studies demonstrate that the expression of all three chitinase family members was significantly increased in airway inflammation induced by ASL volume depletion. However, their distinct temporal regulation in lungs from wild-type and βENaC-overexpressing mice suggests that Ym1, Ym2, and AMCase may have unique functions in pulmonary homeostasis and in the pathogenesis of airway disease.

Na^+ Hyperabsorption Is Associated with Emphysema

Because distal airspaces were enlarged in lungs from adult βENaC-overexpressing mice (11), we performed quantitative longitudinal studies on lung volumes and mean linear intercepts as a parameter for alveolar diameter in lungs ranging from neonatal to adult βENaC-overexpressing and control mice. In histologic sections, alveolar size and architecture were normal at birth, but alveoli were substantially enlarged in 3-week-old and adult βENaC-overexpressing mice versus control mice (Figures 9A–9D). Similarly, lung volumes were normal in βENaC-overexpressing neonates (PN 5) but were increased significantly relative to control mice at the age of 3 weeks and remained enlarged in

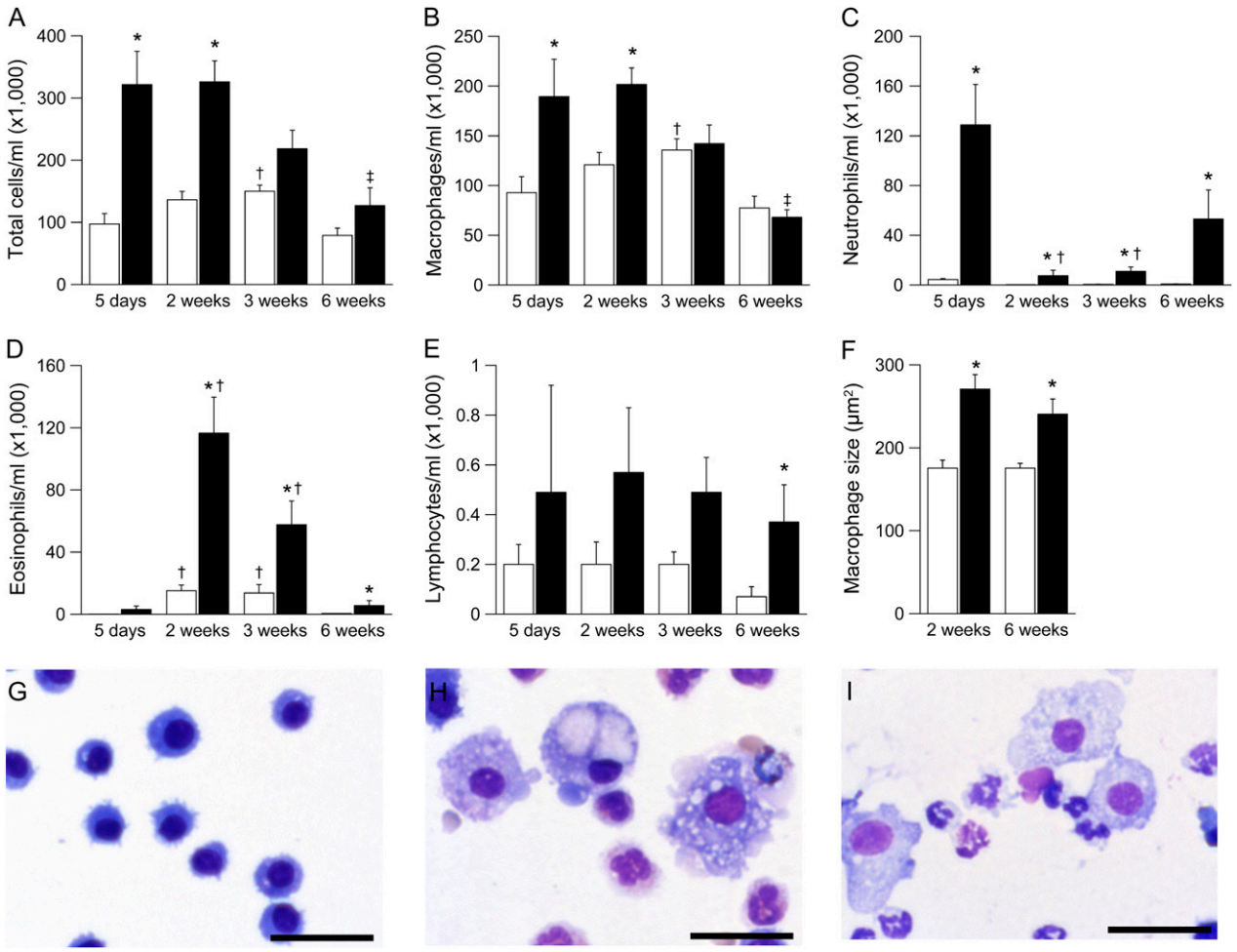

Figure 6. Development of airway inflammation in β-epithelial Na^+ channel (βENaC)-overexpressing mice. (*A–E*) Bronchoalveolar lavage cell counts from wild-type (*open bars*) and βENaC-overexpressing (*solid bars*) mice at 5 days, 2 weeks, 3 weeks, and 6 weeks of age. n = 7–20 mice per group. (*A*) Total cells. *$P < 0.001$ versus wild-type mice of same age; †$P < 0.05$ versus 5-day-old and 6-week-old wild-type mice; ‡$P < 0.05$ versus 5-day-old and 2-week-old βENaC-overexpressing mice. (*B*) Macrophages. *$P < 0.01$ versus wild-type mice of same age; †$P < 0.05$ versus 5-day-old and 6-week-old wild-type mice; ‡$P < 0.05$ versus 5-day-old, 2-week-old, and 3-week-old βENaC-overexpressing mice. (*C*) Neutrophils. *$P < 0.001$ versus wild-type mice of same age; †$P < 0.05$ versus 5-day-old βENaC-overexpressing mice. (*D*) Eosinophils. *$P < 0.001$ versus wild-type mice of same age; †$P < 0.05$ versus 5-day-old and 6-week-old mice of same genotype. (*E*) Lymphocytes. *$P = 0.02$ versus wild-type mice of same age. (*F–I*) Bronchoalveolar macrophages were enlarged (*F*) and morphologically activated in 2-week-old (*H*) and 6-week-old (*I*) βENaC-overexpressing mice compared with wild-type littermates (*G*) (May-Grünwald-Giemsa staining; *scale bars*, 50 μm). *$P < 0.01$ versus littermate control mice.

adult βENaC-overexpressing mice compared with control mice (Figure 9E). Mean linear intercepts were normal at birth but failed to become smaller in 3- and 6-week-old βENaC-overexpressing mice (Figure 9F).

Assessment of pulmonary mechanics by invasive pulmonary function testing in adult mice revealed that the dynamic compliance was significantly increased in adult βENaC-overexpressing mice compared with control mice (Figure 9H). Pressure–volume curves were also shifted to the left in adult βENaC-overexpressing mice, reflecting a significantly increased static compliance compared with wild-type littermates (Figures 9I and 9J). Taken together, these morphologic and functional data demonstrate that ASL depletion causes pulmonary emphysema that evolves in parallel to airway mucus obstruction and inflammation in βENaC-overexpressing mice.

DISCUSSION

This longitudinal characterization of the evolution of lung disease in βENaC-overexpressing mice *in vivo* revealed sequential pathogenetic events in airways disease caused by airway Na^+ hyperabsorption and ASL dehydration. Our morphometric studies defined severe airway mucus obstruction in the first days of life as the earliest and death-causing lesion in βENaC-overexpressing mice. The initial mucus plugging was restricted to the trachea and occurred in the absence of goblet cell metaplasia and elevated mucin gene expression compared with wild-type mice (*see* Figures 1–3ʷ). These results indicate that Na^+ hyperabsorption-induced mucus accumulation was caused by deficient clearance of constitutively secreted mucus and demonstrate that ASL depletion alone (i.e., in the absence of mucus hypersecretion) is sufficient to cause severe airway mucus obstruction with airflow limitation resulting in systemic hypoxia and pulmonary mortality.

The striking similarity between initial mucus plugging in βENaC-overexpressing neonatal mice and infants with CF (27), both exhibiting severe mucus plugging in the absence of goblet cell metaplasia and mucus hypersecretion, indicates that dehydration of airway surfaces may be sufficient to cause severe airway obstruction in the human lung. The regional differences in initial mucus plug formation between βENaC-overexpressing

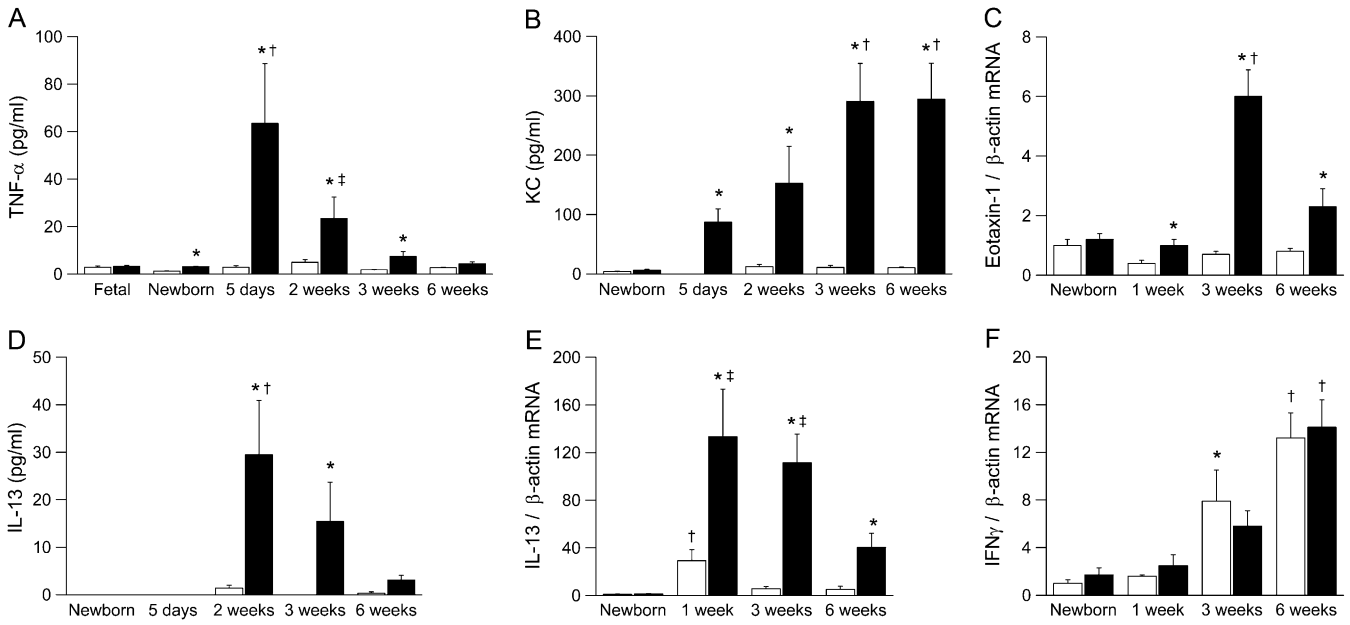

Figure 7. Time course of expression of proinflammatory cytokines in lungs from β-epithelial Na^+ channel (βENaC)-overexpressing mice. (*A–F*) Expression of tumor necrosis factor (TNF)-α, keratinocyte-derived cytokine (KC), eotaxin-1, IL-13, and IFN-γ protein and mRNA in bronchoalveolar lavage and lung homogenates from fetal, newborn, 5-day-old, 2-week-old, 3-week-old, and 6-week-old wild-type (*open bars*) and βENaC-overexpressing (*solid bars*) mice. Data are expressed as absolute protein concentrations or fold changes of transcript expression normalized newborn wild-type mice. n = 5–13 mice per group. (*A*) TNF-α. $*P < 0.01$ versus wild-type mice of same age; $^{\dagger}P < 0.05$ versus newborn βENaC-overexpressing mice; $^{\ddagger}P < 0.05$ versus fetal and newborn βENaC-overexpressing mice. (*B*) KC. $*P < 0.01$ versus wild-type mice of same age; $^{\dagger}P < 0.05$ versus newborn βENaC-overexpressing mice. (*C*) Eotaxin-1 mRNA. $*P < 0.01$ versus wild-type mice of same age; $^{\dagger}P < 0.05$ versus newborn and 1-week-old wild-type mice. (*D*) IL-13. $*P < 0.05$ versus wild-type mice of same age; $^{\dagger}P < 0.05$ versus newborn and 5-day-old, βENaC-overexpressing mice. (*E*) IL-13 mRNA. $*P < 0.05$ versus wild-type mice of same age; $^{\dagger}P < 0.05$ versus newborn and 6-week-old wild-type mice; $^{\ddagger}P < 0.05$ versus newborn βENaC-overexpressing mice. (*F*) IFN-γ mRNA. $*P < 0.05$ versus newborn wild-type mice; $^{\dagger}P < 0.05$ versus newborn and 1-week-old mice of same genotype.

mice and patients with CF, in whom mucus plugging is not restricted to the trachea but is observed initially in the small airways, may reflect species differences in the anatomic structure of the tracheobronchial tree. In mice, due to the paucity of airway branching, the narrowest cross-sectional surface area of the tracheobronchial tree is found at the level of the trachea, whereas the extensive branching of human airways produces significant restrictions in surface area at the level of the terminal bronchiole (28). Accordingly, the locus of initial mucus plaque formation in infants with CF and neonatal βENaC-overexpressing mice is consistent with the concept that ASL volume depletion–induced mucus obstruction occurs in regions of the tracheobronchial tree with critical reductions of total airway caliber. Alternatively, the observed differences in localization of early mucus plugging between patients with CF and βENaC-overexpressing mice may be related to regional differences in relative expression of abnormal Na^+ transport, goblet cell numbers, and/or mucin secretory rates.

The histopathologic search for early changes in the intrapulmonary airways revealed that epithelial cells of βENaC-overexpressing neonates were depleted of glycogen stores and that a subset of cells subsequently underwent hydropic degeneration and necrosis in the absence of detectable intrapulmonary mucus obstruction (Figure 4). The following observations suggest that epithelial necrosis is a direct consequence of increased airway Na^+ absorption. First, glycogen depletion and epithelial degeneration were confined to CCSP-positive Clara cells (i.e., the cell type in which CCSP-driven overexpression of βENaC was induced). Second, epithelial degeneration was not observed in airways from mice that overexpressed αENaC or γENaC and did not exhibit increased airway Na^+ absorption (data not shown). Third, previous studies in human CF airways demonstrated that increased airway Na^+ absorption caused increased epithelial energy consumption (29). Collectively, these data suggest that reduced oxygen tension due to formation of tracheal mucus plugs in the first days of life (*see* Figure 1 and Table 1), coupled with increased O_2 demands of βENaC-overexpressing Clara cells, produced cellular hypoxia (Figure 5) that resulted in necrotic degeneration of a susceptible cell population (likely Clara cells) in βENaC-overexpressing neonates.

We speculate that release of proinflammatory stimuli by necrotic epithelial cells played a key role in the recruitment of macrophages and in the initiation of airway inflammation in neonatal βENaC-overexpressing mice (Figures 4, 6, and 7). Macrophages are a major source of TNF-α, which acts as a potent proinflammatory cytokine in the lung. Therefore, Na^+ hyperabsorption–induced epithelial necrosis generated a previously unrecognized trigger for an inflammatory response (30). Such a mechanism could contribute to early inflammation observed in a number of infants with CF in the absence of detectable bacterial infection. Although necrosis is not a commonly mentioned feature of CF pathogenesis, ultrastructural studies have detected necrotic debris in the small airways of patients with CF in the absence of bacterial infection (31).

In addition to macrophage recruitment and elevation of TNF-α, the initial inflammatory response caused by ASL depletion was dominated by an elevation of airway neutrophils and the neutrophil chemoattractant KC, as previously described for adult βENaC-overexpressing mice (11) (Figures 6 and 7). Juvenile βENaC-overexpressing mice also exhibited a transient airway eosinophilia and increased expression of the key Th2 signaling molecule IL-13 that was markedly exaggerated as com-

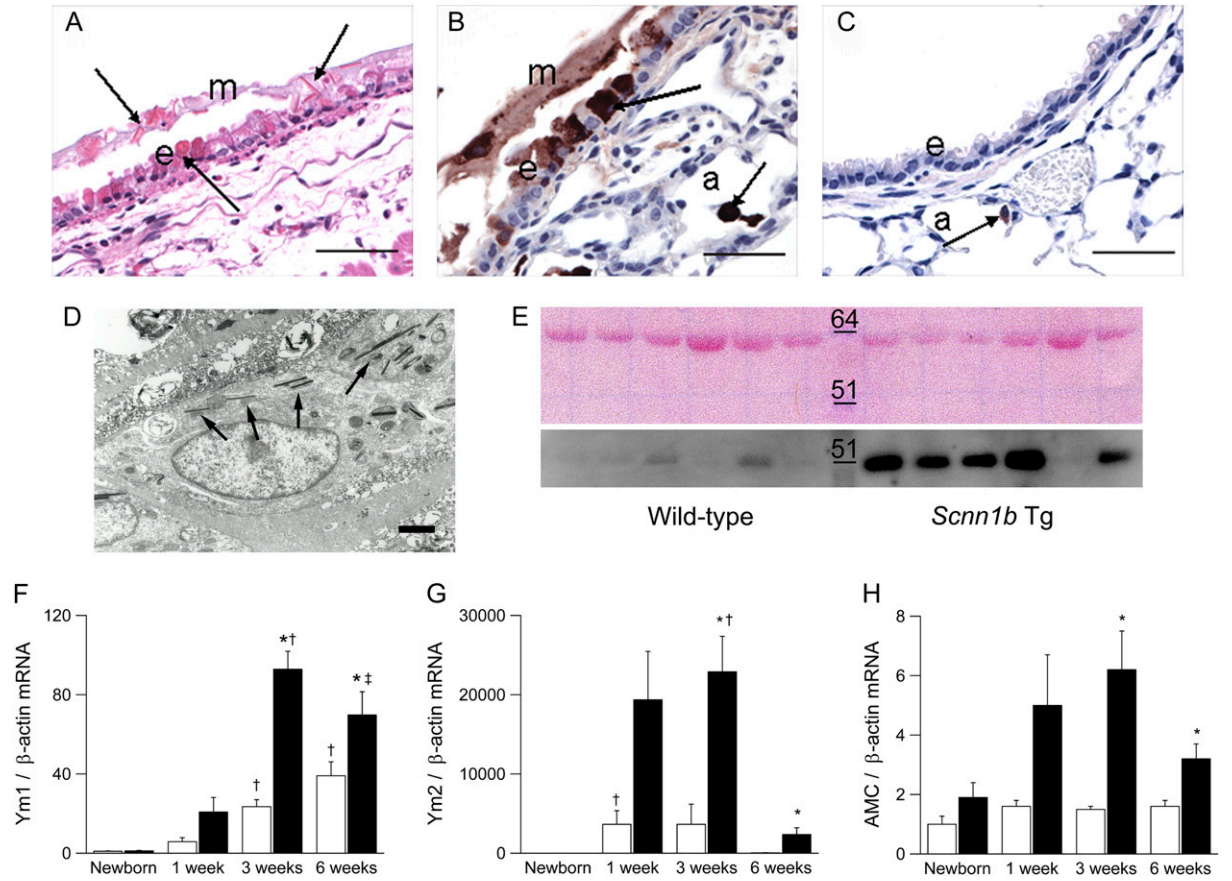

Figure 8. Pulmonary expression of chitinases in β-epithelial Na^+ channel (βENaC)-overexpressing mice. (*A*) Eosinophilic crystals in airway epithelium and overlying mucus and intracytoplasmatic material in nonciliated epithelial cells (*arrows*) in a large-diameter main axial airway from a βENaC-overexpressing mouse (hematoxylin and eosin). e = Epithelium; m = mucus, *scale bar*, 50 μm. (*B, C*) Immunolocalization with polyclonal antibody for Ym1 showing strong Ym1 staining in airway mucus, nonciliated epithelial cells, and alveolar macrophages (*arrows*) of βENaC-overexpressing mice (*B*). a = Alveoli. (*C*) In wild-type mice, weak Ym1-positive staining was limited to alveolar macrophages (*arrow*). *Scale bars*, 25 μm. (*D*) Transmission electron microscopy of a macrophage in the airway lumen from a βENaC-overexpressing mouse containing intracellular electron-dense crystals (*arrows*). *Scale bar*, 2.5 μm. (*E*) Western blot for AMCase in bronchoalveolar lavage from wild-type and βENaC-overexpressing mice. *Upper panel*: Membrane stained with Ponceau S to control for equivalent loading (~60 kD band likely represents albumin). *Lower panel*: AMCase (molecular weight ~52 kD) is more abundant in bronchoalveolar lavage fluid from βENaC-overexpressing mice than in wild-type littermates. Representative for n = 6–8 mice per group. (*F–H*) Expression levels of Ym1, Ym2, and AMCase transcripts in lungs from wild-type (*open bars*) and βENaC-overexpressing (*solid bars*) mice at birth, 1 week, 3 weeks, and 6 weeks of age. Data are expressed as fold changes from newborn wild-type mice. n = 6–14 mice per group. (*F*) Ym1 mRNA. $*P < 0.05$ versus wild-type mice of same age; $^{\dagger}P < 0.05$ versus newborn and 1-week-old mice of same genotype; $^{\ddagger}P < 0.05$ versus newborn βENaC-overexpressing mice. (*G*) Ym2 mRNA. $*P < 0.001$ versus wild-type mice of same age; $^{\dagger}P < 0.05$ versus newborn and 6-week-old mice of same genotype. (*H*) AMCase mRNA. $*P < 0.01$ versus wild-type mice of same age.

pared with wild-type animals (32–34). In wild-type and βENaC-overexpressing mice, eosinophil numbers in BALF and IL-13 waned with age, followed by an increase in pulmonary mRNA expression of the Th1 cytokine IFN-γ. Consistent with the data of George and colleagues (23), our data suggest that the immune system of juvenile wild-type mice during normal development is temporarily biased/polarized toward a Th2 response (24). To our knowledge, these are the first data demonstrating that ASL depletion, in addition to producing chronic airway neutrophilia, exaggerates Th2-driven airway inflammation in a Th2-biased host. We propose that ASL depletion impaired clearance of inhaled airborne allergens and triggered Th2-driven inflammation in young βENaC-overexpressing mice. Release of IL-13, which induced expression of eotaxin-1, resulted in the recruitment of eosinophils into the lung (35).

The chronic lung disease in adult βENaC-overexpressing mice, including airway mucus plugging, goblet cell metaplasia, epithelial hypertrophy, elevated mucin gene expression, and airway neutrophilia, persisted after necrotic cells were detectable and Th2-dependent mechanisms waned (Figures 2, 3, 6, and 7). In this context, the present study supports the idea that ASL depletion–induced goblet cell metaplasia and mucus hypersecretion are secondary changes that develop in parallel to, or consequent to, persistent airway inflammation (11, 36, 37). The mechanisms of persistent neutrophilic inflammation and goblet cell metaplasia are not known. We previously hypothesized that chronic airway inflammation and mucus hypersecretion may be perpetuated by a failure to clear inhaled environmental particles and irritants triggering the release of proinflammatory chemokines like MIP-2 and KC from macrophages and/or airway epithelia in βENaC-overexpressing mice (11, 38). We predict that future studies in which βENaC-overexpressing mice are exposed to defined intrapulmonary doses of particulates will help to further elucidate the relative role of air pollution in the pathogenesis of chronic obstructive lung disease caused by ASL depletion and reduced mucus clearance.

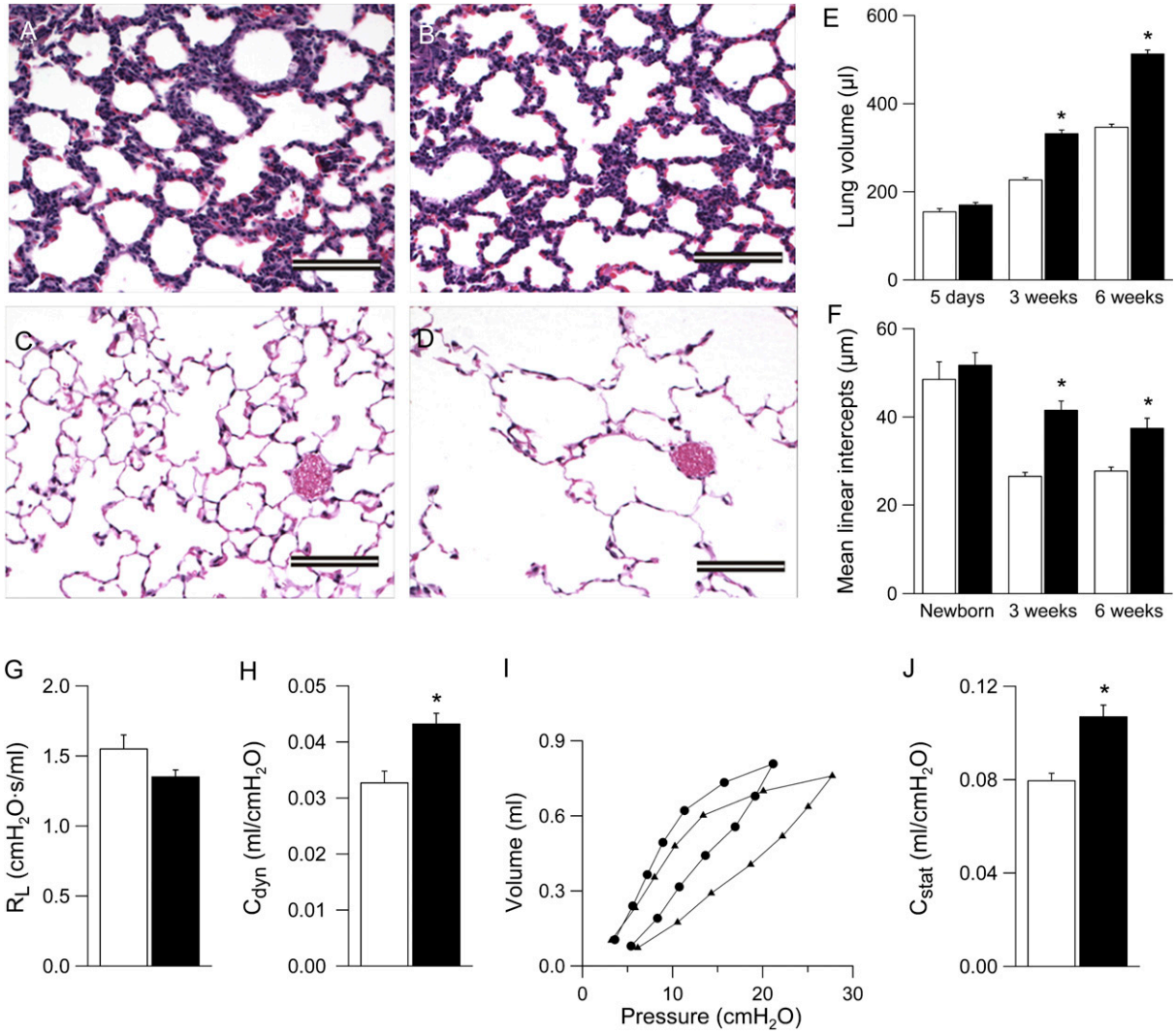

Figure 9. Development of emphysema in β-epithelial Na^+ channel (βENaC)-overexpressing mice. (*A–D*) Lung histology (hematoxylin and eosin) from newborn (*A, B*) and 6-week-old (*C, D*) wild-type (*A, C*), and βENaC-overexpressing (*B, D*) mice. *Scale bars*, 100 μm. (*E, F*) Lung volume (*E*) and mean linear intercepts (*F*) in neonatal to adult βENaC-overexpressing mice (*solid bars*) and wild-type control mice (*open bars*). n = 5–12 mice per group. *$P < 0.001$ versus wild-type mice of same age. (*G*) Pulmonary resistance (R_L), (*H*) dynamic compliance (C_{dyn}), (*I*) pressure–volume curves, and (*J*) static compliance (C_{stat}) were measured in adult βENaC-overexpressing mice (*solid bars* in *G*, *H*, and *J*; *circles* in *I*) and littermate control mice (*open bars* in *G*, *H*, and *J*; *triangles* in *I*). n = 8–14 mice per group. *$P < 0.001$ versus littermate control mice.

Chronic airway inflammation in βENaC-overexpressing mice was also associated with the formation of eosinophilic crystals and increased expression of various members of a recently identified family of mammalian chitinases and chitinase-like proteins, including Ym1, Ym2, and AMCase (18, 19, 25, 26) (Figure 8). Early studies of these proteins in the lung identified elevated expression of Ym1 in mouse models with chronic granulomatous disease, where Ym1 was shown to be a neutrophil granule protein, and it was suggested that crystal formation was due to excess neutrophil turnover at sites of inflammation (25). Subsequently, Ym1 was detected in alveolar macrophages from wild-type mice (39). Recent studies supported the involvement of these chitinases in airway inflammation by demonstrating that (*1*) all three proteins are up-regulated in the context of Th2-driven airway inflammation, (*2*) AMCase expression is elevated in lungs from patients with asthma, and (*3*) AMCase polymorphisms are associated with human asthma (19, 26, 40, 41). Because chitin is expressed in the walls of fungi and parasites and chitinases are expressed in alveolar macrophages, neutrophils, and the airway epithelium, it is possible that chitinases take part in the innate immune defense against these pathogens (42). Conversely, high expression of chitinases during inflammation may have deleterious effects, as indicated by studies showing that inhibition of AMCase activity ameliorates disease severity in murine asthma models (19). Indeed, precipitation and formation of crystals, frequently greater that 100 μm in size, in the airways of βENaC-overexpressing mice may cause mechanical injury of epithelial cells and phagocytes and thus promote chronic inflammation. Although the focus of recent studies on the role of chitinases in airway disease has been on classic Th2-driven inflammatory models, our studies suggest that alternative stimuli (e.g., dehydration) can promote chitinase crystal formation.

Our longitudinal studies demonstrate for the first time that increased airway Na^+ absorption and ASL depletion cause emphysema (Figure 9). Although lung volumes, alveolar architecture, and alveolar size were normal in βENaC-overexpressing neonates, the subsequent increase in lung volume and relative distal airspace enlargement together with an increase in lung

compliance show that βENaC-overexpressing mice develop emphysema in the first weeks of life.

We speculate that several mechanisms may contribute to the development of emphysema *in vivo* in βENaC-overexpressing mice (Figure 9). First, emphysema in adult βENaC-overexpressing mice may reflect failure of alveolar septation during development. Because overexpression of βENaC under control of the CCSP promoter is turned on several days before birth (43), increased pulmonary Na^+ absorption in the prenatal period may cause a slight deflation of the lungs with reduced transpulmonary pressure, which may reduce a stimulus for postnatal growth of alveolar walls. Second, the observation that lungs seem to be consistently hyperinflated even in the absence of constant pressure fixation indicates that early airway mucus plugging caused persistent air-trapping, which may result in mechanical overdistention of distal airspaces with irreversible disruption of alveolar septi, loss of pulmonary elastance, and alveolar remodeling. Third, it is possible that chronic pulmonary inflammation contributes to the development of emphysema in βENaC-overexpressing mice. Several leukocyte-derived proteases, including neutrophil elastase and macrophage elastase, have been shown to cause emphysema in mice (44–46). Previous studies demonstrated that overexpression of several proinflammatory mediators, including TNF-α and IL-13, in genetically modified mice causes an imbalance in the pulmonary protease/antiprotease system and emphysema (47, 48) and indicated that proteases/antiproteases may play a key role during lung development (49). Because TNF-α, IL-13, and neutrophils are increased and macrophages are morphologically activated in the lungs of βENaC-overexpressing mice, we speculate that disruption of the protease/antiprotease balance in the developing lung may cause ASL depletion–induced emphysema. Although further dissection of the relative roles of these mechanisms and their relationship to airway Na^+ hyperabsorption is required, it is noteworthy that emphysema, together with mucus plugging, constitutes an early and invariable feature in the CF lung (27). Recent studies indicated that improvement of ASL hydration by preventive treatment with the specific ENaC blocker amiloride can reduce mortality, airway inflammation, and airway mucus obstruction in βENaC-overexpressing mice (50). Future studies are required to determine if improved hydration of airway surfaces can prevent emphysema formation in βENaC-overexpressing mice.

On the basis of the similarities in the pulmonary phenotype between adult βENaC-overexpressing mice and chronic bronchitis, including airway mucus obstruction, goblet cell metaplasia, chronic inflammation, and emphysema (51), we speculate that ASL depletion may play a critical role in the pathogenesis of reduced mucus clearance observed in the airways of smokers and patients with chronic bronchitis (52, 53). In contrast to CF, no intrinsic ion transport abnormalities have been reported in airways from patients with chronic bronchitis. However, cigarette smoke has been shown to decrease CFTR expression and cAMP-dependant Cl^- secretion in airway epithelia *in vitro* and *in vivo* (12, 54), providing a mechanism for ASL depletion. Furthermore, cigarette smoke induces hypersecretion of mucin macromolecules. In the presence of limited ion transport compensation (55), the mucins secreted "dry" onto airway surfaces (56–58) are not properly hydrated, producing "secondary" ASL depletion. The ASL depletion consequent to both mechanisms would be predicted to produce the slow mucus clearance and mucus adhesion characteristic of COPD (52, 53).

The observation that ASL depletion can cause concomitant neutrophilic and Th2-driven airway inflammation is remarkable in the context of the debate over whether COPD and asthma are distinct disease entities, as proposed by the "British hypothesis," or whether they are based on a common etiologic background, as put forward by the "Dutch hypothesis" (59). Our results point to the possibility of a single etiologic hypothesis for seemingly diverse chronic obstructive airway diseases, including CF, COPD, and asthma, in which a defect in mechanical clearance of inhaled particulates, allergens, or pathogens, caused by primary or secondary ASL depletion, plays a critical role in disease pathogenesis. In this context, the interplay between deficient mechanical lung clearance and the host immune response determines whether a stimulus triggers a neutrophil-dominated airway disease, a Th2-driven airway disease, or both.

In summary, the longitudinal evaluation of the spontaneous course of lung disease in βENaC-overexpressing mice provides novel insights into the *in vivo* pathogenesis of chronic obstructive lung disease. First, we show that ASL depletion is sufficient to initiate severe airway mucus obstruction in the absence of goblet cell metaplasia or mucus hypersecretion. Second, we show that airway mucus plugging/hypoxia is associated with epithelial necrosis, constituting a mechanism to initiate airway inflammation in the absence of infection. Third, we demonstrate that ASL depletion causes exaggerated eosinophilic airway inflammation in a Th2-biased host. Finally, we show that increased airway Na^+ absorption can cause emphysema. Taken together, these results suggest that deficient airway surface hydration plays a critical role in the pathogenesis and serves as a novel therapeutic target in of chronic obstructive pulmonary diseases of different etiologies.

Conflict of Interest Statement: M.A.M is listed on a patent application filed by the University of North Carolina at Chapel Hill, describing the βENaC-overexpressing mouse. The βENaC-overexpressing mouse has been deposited at JAX for general disposition. J.R.H. does not have a financial relationship with a commercial entity that has an interest in the subject of this manuscript. J.B.T. does not have a financial relationship with a commercial entity that has an interest in the subject of this manuscript. D.T. does not have a financial relationship with a commercial entity that has an interest in the subject of this manuscript. A.L. does not have a financial relationship with a commercial entity that has an interest in the subject of this manuscript. S.S. does not have a financial relationship with a commercial entity that has an interest in the subject of this manuscript. Z.Z. does not have a financial relationship with a commercial entity that has an interest in the subject of this manuscript. S.M.K. does not have a financial relationship with a commercial entity that has an interest in the subject of this manuscript. S.L.T. does not have a financial relationship with a commercial entity that has an interest in the subject of this manuscript. E.J.H. does not have a financial relationship with a commercial entity that has an interest in the subject of this manuscript. W.K.O. does not have a financial relationship with a commercial entity that has an interest in the subject of this manuscript. R.C.B. is listed on a patent application filed by the University of North Carolina at Chapel Hill describing the βENaC-overexpressing mouse.

Acknowledgment: The authors thank Lori Bramble, Brian Brighton, Kim Burns, Ralph Common, Brigitte Häusle-Vior, Stephanie Hirtz, Michelle Perry, Amy Porter, and Jolanthe Schatterny for expert technical assistance; Lisa Brown for editing of the manuscript; and Dr. Andreas Kulozik for general support.

References

1. Kerem B, Rommens JM, Buchanan JA, Markiewicz D, Cox TK, Chakravarti A, Buchwald M, Tsui LC. Identification of the cystic fibrosis gene: genetic analysis. *Science* 1989;245:1073–1080.
2. Welsh MJ, Ramsey BW, Accurso F, Cutting GR. Cystic fibrosis. In: Scriver CR, Beaudet AL, Sly WS, and Valle D, editors. The metabolic and molecular bases of inherited disease, 8th ed. New York: McGraw-Hill; 2001. pp. 5121–5188.
3. Anderson MP, Gregory RJ, Thompson S, Souza DW, Paul S, Mulligan RC, Smith AE, Welsh MJ. Demonstration that CFTR is a chloride channel by alteration of its anion selectivity. *Science* 1991;253:202–205.
4. Canessa CM, Schild L, Buell G, Thorens B, Gautschl I, Horisberger JD, Rossier BC. Amiloride-sensitive epithelial Na^+ channel is made of three homologous subunits. *Nature* 1994;367:463–467.
5. Stutts MJ, Canessa CM, Olsen JC, Hamrick M, Cohn JA, Rossier BC, Boucher RC. CFTR as a cAMP-dependent regulator of sodium channels. *Science* 1995;269:847–850.

6. Mall M, Hipper A, Greger R, Kunzelmann K. Wild type but not ΔF508 CFTR inhibits Na^+ conductance when coexpressed in *Xenopus* oocytes. *FEBS Lett* 1996;381:47–52.
7. Knowles MR, Stutts MJ, Spock A, Fischer N, Gatzy JT, Boucher RC. Abnormal ion permeation through cystic fibrosis respiratory epithelium. *Science* 1983;221:1067–1070.
8. Boucher RC, Stutts MJ, Knowles MR, Cantley L, Gatzy JT. Na+ transport in cystic fibrosis respiratory epithelia: abnormal basal rate and response to adenylate cyclase activation. *J Clin Invest* 1986;78: 1245–1252.
9. Mall M, Bleich M, Greger R, Schreiber R, Kunzelmann K. The amiloride inhibitable Na+ conductance is reduced by CFTR in normal but not in cystic fibrosis airways. *J Clin Invest* 1998;102:15–21.
10. Matsui H, Grubb BR, Tarran R, Randell SH, Gatzy JT, Davis CW, Boucher RC. Evidence for periciliary liquid layer depletion, not abnormal ion composition, in the pathogenesis of cystic fibrosis airways disease. *Cell* 1998;95:1005–1015.
11. Mall M, Grubb BR, Harkema JR, O'Neal WK, Boucher RC. Increased airway epithelial Na^+ absorption produces cystic fibrosis-like lung disease in mice. *Nat Med* 2004;10:487–493.
12. Cantin AM, Hanrahan JW, Bilodeau G, Ellis L, Dupuis A, Liao J, Zielenski J, Durie P. Cystic fibrosis transmembrane conductance regulator function is suppressed in cigarette smokers. *Am J Respir Crit Care Med* 2006;173:1139–1144.
13. Livraghi A, O'Neal WK, Mall M, Boucher RC. Airway inflammation in Scnn1b transgenic mice [abstract]. *Pediatr Pulmonol Suppl* 2005; 28:261.
14. Mall MA, Harkema JR, Trojanek J, Treis D, Schubert S, Zhou Z, Tilley SL, Livraghi A, O'Neal WK, Boucher RC. Initial pulmonary lesions and spontaneous course of lung disease caused by airway surface liquid depletion in βENaC overexpressing mice [abstract]. *Pediatr Pulmonol Suppl* 2007;30:279–280.
15. Harkema JR, Plopper CG, Hyde DM, St George JA. Regional differences in quantities of histochemically detectable mucosubstances in nasal, paranasal, and nasopharyngeal epithelium of the bonnet monkey. *J Histochem Cytochem* 1987;35:279–286.
16. Scherle W. A simple method for volumetry of organs in quantitative stereology. *Mikroskopie* 1970;26:57–60.
17. Dunnill MS. Quantitative methods in the study of pulmonary pathology. *Thorax* 1962;17:320–328.
18. Ward JM, Yoon M, Anver MR, Haines DC, Kudo G, Gonzalez FJ, Kimura S. Hyalinosis and Ym1/Ym2 gene expression in the stomach and respiratory tract of 129S4/SvJae and wild-type and CYP1A2-null B6, 129 mice. *Am J Pathol* 2001;158:323–332.
19. Zhu Z, Zheng T, Homer RJ, Kim YK, Chen NY, Cohn L, Hamid Q, Elias JA. Acidic mammalian chitinase in asthmatic Th2 inflammation and IL-13 pathway activation. *Science* 2004;304:1678–1682.
20. Pfaffl MW. A new mathematical model for relative quantification in real-time RT-PCR. *Nucleic Acids Res* 2001;29:E45.
21. Hartney JM, Coggins KG, Tilley SL, Jania LA, Lovgren AK, Audoly LP, Koller BH. Prostaglandin E2 protects lower airways against bronchoconstriction. *Am J Physiol Lung Cell Mol Physiol* 2006;290: L105–L113.
22. Lovgren AK, Jania LA, Hartney JM, Parsons KK, Audoly LP, Fitzgerald GA, Tilley SL, Koller BH. COX-2-derived prostacyclin protects against bleomycin-induced pulmonary fibrosis. *Am J Physiol Lung Cell Mol Physiol* 2006;291:L144–L156.
23. George CL, White ML, Kulhankova K, Mahajan A, Thorne PS, Snyder JM, Kline JN. Early exposure to a nonhygienic environment alters pulmonary immunity and allergic responses. *Am J Physiol Lung Cell Mol Physiol* 2006;291:L512–L522.
24. Adkins B, Leclerc C, Marshall-Clarke S. Neonatal adaptive immunity comes of age. *Nat Rev Immunol* 2004;4:553–564.
25. Harbord M, Novelli M, Canas B, Power D, Davis C, Godovac-Zimmermann J, Roes J, Segal AW. Ym1 is a neutrophil granule protein that crystallizes in p47phox-deficient mice. *J Biol Chem* 2002;277: 5468–5475.
26. Webb DC, McKenzie AN, Foster PS. Expression of the Ym2 lectin-binding protein is dependent on interleukin (IL)-4 and IL-13 signal transduction: identification of a novel allergy-associated protein. *J Biol Chem* 2001;276:41969–41976.
27. Zuelzer WW, Newton WA. The pathogenesis of fibrocystic disease of the pancreas: a study of 36 cases with special reference to the pulmonary lesions. *Pediatrics* 1949;4:53–69.
28. Weibel ER. Morphometry of the human lung. Berlin: Springer Verlag; 1963.
29. Stutts MJ, Knowles MR, Gatzy JT, Boucher RC. Oxygen consumption and ouabain binding sites in cystic fibrosis nasal epithelium. *Pediatr Res* 1986;20:1316–1320.
30. Chen CJ, Kono H, Golenbock D, Reed G, Akira S, Rock KL. Identification of a key pathway required for the sterile inflammatory response triggered by dying cells. *Nat Med* 2007;13:851–856.
31. Simel DL, Mastin JP, Pratt PC, Wisseman CL, Shelburne JD, Spock A, Ingram P. Scanning electron microscopic study of the airways in normal children and in patients with cystic fibrosis and other lung diseases. *Pediatr Pathol* 1984;2:47–64.
32. Wills-Karp M, Luyimbazi J, Xu X, Schofield B, Neben TY, Karp CL, Donaldson DD. Interleukin-13: central mediator of allergic asthma. *Science* 1998;282:2258–2261.
33. Grunig G, Warnock M, Wakil AE, Venkayya R, Brombacher F, Rennick DM, Sheppard D, Mohrs M, Donaldson DD, Locksley RM, *et al.* Requirement for IL-13 independently of IL-4 in experimental asthma. *Science* 1998;282:2261–2263.
34. Zhu Z, Homer RJ, Wang Z, Chen Q, Geba GP, Wang J, Zhang Y, Elias JA. Pulmonary expression of interleukin-13 causes inflammation, mucus hypersecretion, subepithelial fibrosis, physiologic abnormalities, and eotaxin production. *J Clin Invest* 1999;103:779–788.
35. Rothenberg ME, Hogan SP. The eosinophil. *Annu Rev Immunol* 2006;24:147–174.
36. Takeyama K, Agusti C, Ueki I, Lausier J, Cardell LO, Nadel JA. Neutrophil-dependent goblet cell degranulation: role of membrane-bound elastase and adhesion molecules. *Am J Physiol* 1998;275:L294–L302.
37. Voynow JA, Young LR, Wang Y, Horger T, Rose MC, Fischer BM. Neutrophil elastase increases MUC5AC mRNA and protein expression in respiratory epithelial cells. *Am J Physiol* 1999;276:L835–L843.
38. Fujii T, Hayashi S, Hogg JC, Vincent R, Van Eeden SF. Particulate matter induces cytokine expression in human bronchial epithelial cells. *Am J Respir Cell Mol Biol* 2001;25:265–271.
39. Nio J, Fujimoto W, Konno A, Kon Y, Owhashi M, Iwanaga T. Cellular expression of murine Ym1 and Ym2, chitinase family proteins, as revealed by in situ hybridization and immunohistochemistry. *Histochem Cell Biol* 2004;121:473–482.
40. Homer RJ, Zhu Z, Cohn L, Lee CG, White WI, Chen S, Elias JA. Differential expression of chitinases identify subsets of murine airway epithelial cells in allergic inflammation. *Am J Physiol Lung Cell Mol Physiol* 2006;291:L502–L511.
41. Bierbaum S, Nickel R, Koch A, Lau S, Deichmann KA, Wahn U, Superti-Furga A, Heinzmann A. Polymorphisms and haplotypes of acid mammalian chitinase are associated with bronchial asthma. *Am J Respir Crit Care Med* 2005;172:1505–1509.
42. Reese TA, Liang HE, Tager AM, Luster AD, Van Rooijen N, Voehringer D, Locksley RM. Chitin induces accumulation in tissue of innate immune cells associated with allergy. *Nature* 2007;447:92–96.
43. Hackett BP, Gitlin JD. 5′ Flanking region of the Clara cell secretory protein gene specifies a unique temporal and spatial pattern of gene expression in the developing pulmonary epithelium. *Am J Respir Cell Mol Biol* 1994;11:123–129.
44. Shapiro SD, Goldstein NM, Houghton AM, Kobayashi DK, Kelley D, Belaaouaj A. Neutrophil elastase contributes to cigarette smoke-induced emphysema in mice. *Am J Pathol* 2003;163:2329–2335.
45. Hautamaki RD, Kobayashi DK, Senior RM, Shapiro SD. Requirement for macrophage elastase for cigarette smoke-induced emphysema in mice. *Science* 1997;277:2002–2004.
46. Churg A, Wright JL. Proteases and emphysema. *Curr Opin Pulm Med* 2005;11:153–159.
47. Fujita M, Shannon JM, Irvin CG, Fagan KA, Cool C, Augustin A, Mason RJ. Overexpression of tumor necrosis factor-alpha produces an increase in lung volumes and pulmonary hypertension. *Am J Physiol Lung Cell Mol Physiol* 2001;280:L39–L49.
48. Zheng T, Zhu Z, Wang Z, Homer RJ, Ma B, Riese RJ Jr, Chapman HA Jr, Shapiro SD, Elias JA. Inducible targeting of IL-13 to the adult lung causes matrix metalloproteinase- and cathepsin-dependent emphysema. *J Clin Invest* 2000;106:1081–1093.
49. Ryu J, Vicencio AG, Yeager ME, Kashgarian M, Haddad GG, Eickelberg O. Differential expression of matrix metalloproteinases and their inhibitors in human and mouse lung development. *Thromb Haemost* 2005;94:175–183.
50. Zhou Z, Treis D, Schubert S, Harm M, Schatterny J, Hirtz S, Duerr J, Boucher RC, Mall MA. Preventive but not late ENaC blocker therapy reduces mortality and morbidity of cystic fibrosis-like lung disease in mice [abstract]. *Pediatr Pulmonol Suppl* 2007;30:294.

51. Hogg JC, Chu F, Utokaparch S, Woods R, Elliott WM, Buzatu L, Cherniack RM, Rogers RM, Sciurba FC, Coxson HO, *et al.* The nature of small-airway obstruction in chronic obstructive pulmonary disease. *N Engl J Med* 2004;350:2645–2653.
52. Goodman RM, Yergin BM, Landa JF, Golivanux MH, Sackner MA. Relationship of smoking history and pulmonary function tests to tracheal mucous velocity in nonsmokers, young smokers, ex-smokers, and patients with chronic bronchitis. *Am Rev Respir Dis* 1978;117:205–214.
53. Wanner A, Salathe M, O'Riordan TG. Mucociliary clearance in the airways. *Am J Respir Crit Care Med* 1996;154:1868–1902.
54. Welsh MJ. Cigarette smoke inhibition of ion transport in canine tracheal epithelium. *J Clin Invest* 1983;71:1614–1623.
55. Knowles M, Murray G, Shallal J, Askin F, Ranga V, Gatzy J, Boucher R. Bioelectric properties and ion flow across excised human bronchi. *J Appl Physiol* 1984;56:868–877.
56. Verdugo P. Mucin exocytosis. *Am Rev Respir Dis* 1991;144:S33–S37.
57. Tarran R, Grubb BR, Gatzy JT, Davis CW, Boucher RC. The relative roles of passive surface forces and active ion transport in the modulation of airway surface liquid volume and composition. *J Gen Physiol* 2001;118:223–236.
58. Boucher RC. Relationship of airway epithelial ion transport to chronic bronchitis. *Proc Am Thorac Soc* 2004;1:66–70.
59. Vestbo J, Prescott E. Update on the "Dutch hypothesis" for chronic respiratory disease. *Thorax* 1998;53:S15–S19.